Article

SiO_2 coated up-conversion nanomaterial doped with Ag nanoparticles for Micro-CT imaging

Zhangwei[1], Yanli Lu[1], Yang Zang[1], Jinghui Han[2], Qingyun Xiong[1], Jinping Xiong[1,3*]

[1] Beijing Key Laboratory of Electrochemical Process and Technology of Materials, Beijing University of Chemical Technology, Beijing 100029, People's Republic of China
[2] State Key Laboratory of Organic-Inorganic Composites, Beijing University of Chemical Technology, Beijing 100029, People's Republic of China
[3] College of Ecology and Resources Engineering, Wuyi University, Wuyishan 354300, People's Republic of China

* Correspondence: xiongjp@mail.buct.edu.cn

Abstract: In this study, a new method for synthesizing Ag-$NaYF_4$:Yb^{3+}/Er^{3+}@ SiO_2 nanocomposites was introduced. Using a hydrothermal method, the synthesized Yb^{3+}- and Er^{3+}-codoped $NaYF_4$ upconversion luminescent materials and Ag nanoparticles were doped into upconversion nanomaterials and coated with SiO_2 up-conversion nan6omaterials. This material is known as Ag-UCNPs-SiO_2' it improves both the luminous intensity because of the doped Ag nanoparticles and has low cytotoxicity because of the SiO_2 coating. The morphology of UCNPs was observed using scanning electron microscopy (SEM), and the mapping confirmed the successful doping of Ag nanoparticles. Successful coating of SiO_2 was confirmed using transmission electron microscopy (TEM). Fluorescence spectra were used to compare changes in luminescence intensity before and after doping Ag nanoparticles. The reason for the increase in luminescence intensity after doping with Ag nanoparticles was simulated using first-principles calculations. The cytotoxicity of Ag-UCNPs-SiO_2 was tested via the cell counting kit-8 (CCK-8) method, and its imaging ability was characterized using the micro-CT method.

Keywords: up-conversion; nanomaterials; CT imaging

1. Introduction

Generally, upconversion rare-earth nanomaterials are used in many fields because of their high fluorescence intensity. Recently, their application in biomedicine has been extensively studied. Many researchers proposed that they can be used in biological imaging because they provide considerable advantage in the fight against major diseases such as cancer [1–3]. However, the common limitation is that upconversion rare-earth nanomaterials have insufficient luminous intensity and are toxic to biological cells; therefore, the modification of structure and surface is necessary. To increase luminous intensity, many researchers proposed doping Mo^{3+}, Cu^{2+}, and other metal ions in the $NaYF_4$:Yb^{3+}/ Er^{3+} unit cell; however, the effect is not significant [4–6]. Other studies proposed doping with Ag, which has a significant effect but Ag has a high light-to-heat conversion efficiency and can cause cell apoptosis without targeting; therefore, Ag cannot be used in biological studies [7,8]. Many researchers proposed developing core-shell structures such as $NaYF_4$:Yb^{3+}/Er^{3+}@$NaGdF_4$:Yb^{3+} and $NaYF_4$:Yb^{3+}/Er^{3+}@$NaNdF_4$:Yb^{3+}/Tm^{3+}@$NaGdF_4$:Yb^{3+} [9–11]. Alternatively, the material surface is covered with a biocompatible coating such as DSPE-PEG_{2K} and ICG [12–14]. Although these operations can reduce biological toxicity and meet the basic requirements for use in biological cells or animals, these structures will indeed reduce the luminous

intensity of upconversion luminescent materials [15–17]. If such a material is used as a contrast agent for CT imaging, the image will be unclear; moreover, the tumor cannot be observed and additional diagnosis and treatment will be difficult [18–20]. Therefore, this study proposes a new structural upconversion nanomaterial that has both extremely low cytotoxicity and good luminescence intensity and good targeting that can accurately label tumor cells and can be used for in-vivo imaging and obtain clear tumor images using Micro-CT. This study proposes using the coprecipitation-hydrothermal-reverse microemulsion (CHRm) method to synthesize the core-shell structure of Ag-UCNPs-SiO_2. First, the copolymer of Ag nanoparticles and NaREF4 was obtained using a co-precipitation method. Secondly, this copolymer was transformed to Ag-UCNPs in a hexagonal crystal form using a hydrothermal method. Finally, a SiO_2 layer was coated using a reverse microemulsion method.

2. Experimental

2.1. Materials

Y_2O_3 (99.99%), Yb_2O_3 (99.99%), Er_2O_3 (99.99%), nitric acid (68%), sodium fluoride (99.99%), citric acid (99.99%), cyclohexane (99.5%), sliver nitrate (99.99%), ethylenediaminetetraacetic acid (EDTA, ≥99%), sodium hydroxide (≥98%) and polyethylene pyrrolidone (PVP, average molecular weight of 1000000–1500000) were purchased from Aladdin. The cell counting kit 8 (CCK-8) assay kit was purchased from BOVOGEN. All chemicals were used as-received without additional purification.

2.2. Synthesis of Ag nanoparticles

By dropping, 60 mL of 0.05 mol/L of citric acid solution was added to 3 mL of 0.02 mol/L of $AgNO_3$ to obtain a mixture. Moreover, after 5 min of continuous stirring, the solution was transferred to a 100 mL reactor and placed in an oven for the reaction at 120°C for 6 h. The reaction was then cooled to room temperature, washed, and centrifuged to obtain solid Ag nanoparticles, and then added to 10 mL of deionized water and PVP, and then placed in a test tube to prepare the sol for use.

2.3. Synthesis of Ag-UCNPs

RE_2O_3 (RE = Y, Yb, Er) was heated to achieve complete dissolution in excess nitric acid and then transferred to a vacuum system for evaporation to obtain a solid $RE(NO_3)_3$, which was then dissolved in deionized water and recrystallized twice. A certain amount of solid $RE(NO_3)_3$ was dissolved in deionized water, and EDTA (molar ratio of EDTA: $RE(NO_3)_3$ = 1:1) was added and stirred at 600 rpm for 1 h, the mixture was then weighed and dissolved in sodium fluoride in deionized water by ultrasound, and then the solution was added and stirred at 600 rpm for 1 h. Finally, the pH value was adjusted to 5.5 with NaOH and add 10 ml of sliver, and then place it in a hydrothermal kettle to react at 190°C for 24 h. The reaction products were cooled, centrifuged, and washed twice with ethanol/deionized water (1:1 v/v), and dried in vacuum at 80°C for 3 h. The resultant powder is dispersed in cyclohexane for later use.

2.4. Synthesis of Ag-UCNPs@ SiO_2

Note that 0.0083 g of Ag-UCNPs, 0.1 mL of CO-520 and 10 mL of cyclohexane were mixed and stirred for 10 min. Moreover, 0.4 mL of CO-520 and 0.08 mL of 30 wt% ammonia were added and the container was sealed and sonicated for 20 min until a transparent emulsion was formed. Furthermore, 0.04 mL of TEOS (variable concentration used determined by the distance between AgNPs and $NaYF_4$: Yb, Er) was then added to the solution. The solution was stirred for 48 h at 1000 rpm. Finally, the product was collected by centrifugation, washed with deionized water and ethanol twice, and then re-dispersed in 6.0 mL of ethanol.

2.5. Characterization

Transmission electron microscopy (TEM) measurements were performed on a JEOL 2011 microscope operating at 200 kV. All samples were first dispersed in ethanol and then collected using a Cu grid covered with a carbon film for measurement. To determine the elemental composition of the samples, energy-dispersive X-ray spectroscopy (EDS) of the samples was performed on a JEOL 2010 EDS instrument using high-resolution transmission electron microscopy (HRTEM) measurements. Inductively coupled plasma-atomic emission spectrometry (ICPAES) was performed using a Perkin Elmer 7300DV apparatus. Scanning electron microscopy (SEM) images were obtained using a Philips XL30 electron microscope operating at 20 kV. Before this characterization, a Au film was sprayed on the sample. The upconversion luminescence spectrum was obtained using a spectrum analyzer (ANDO AQ6317, Japan). The sample was placed in a 1.0-cm path length support, which was excited using a 980-nm CW semiconductor diode laser (Pmax 800 mW, 1000 mA). The upconversion luminescence spectrum was obtained by the spectrophotometer using a multimode fiber having a core diameter of 0.6 mm. The distance between the top of the fiber and sample is ~2 mm.

2.6. CCK-8 assay for cytotoxicity

The culture medium in the flask was sucked out, washed with PBS, and then 0.25% of trypsin was added to digest cells after culturing HeLa cells in the logarithmic growth phase. After the removal of trypsin, the DMEM medium containing 10% fetal bovine serum was added to blow the cells, which were then transferred to the sampling tank and blown well. Subsequently, 100 μL cells were injected into a 96-well plate (1×10^4 cells/well) and incubated for 24 h in a constant temperature incubator at 37°C (5% CO_2). The cells were incubated for 1.5 h in an incubator at 37°C with 5% CO_2 in accordance with concentrations of 200, 300, 400, 500, and 600 μg/mL. The culture medium was blotted out, PBS was rinsed twice, the culture medium was replaced in the 96-well plates with 100 μL of fresh DMEM containing 10% fetal bovine serum, and then 10 μL of CCK-8 solution was added to each well. The absorbance of each well at 450 nm was measured using a microplate reader after 2 h of culturing in the incubator. The cell survival rate calculation formula is as follows:

$$\text{Cell survival rate (\%)} = (\text{A sample})/(\text{A control}) \times 100\%$$

3. Results and Discussion

The TEM images of Ag nanoparticles (Fig. 1) prepared using the hydrothermal method show that they are spherical and have an average diameter of ~30 nm. The UV-visible absorption spectra of Ag nanoparticles (Fig. 2) obtained using a UV absorption spectrophotometer shows that the absorption peak of Ag nanoparticles is located at 430 nm, which is consistent with the results reported in the literature.

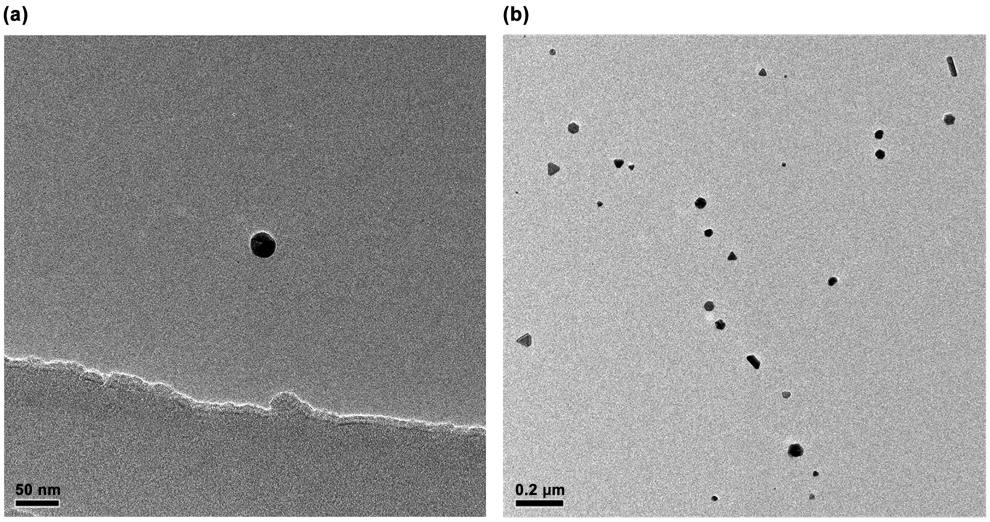

Figure 1. TEM image of Ag nanoparticles

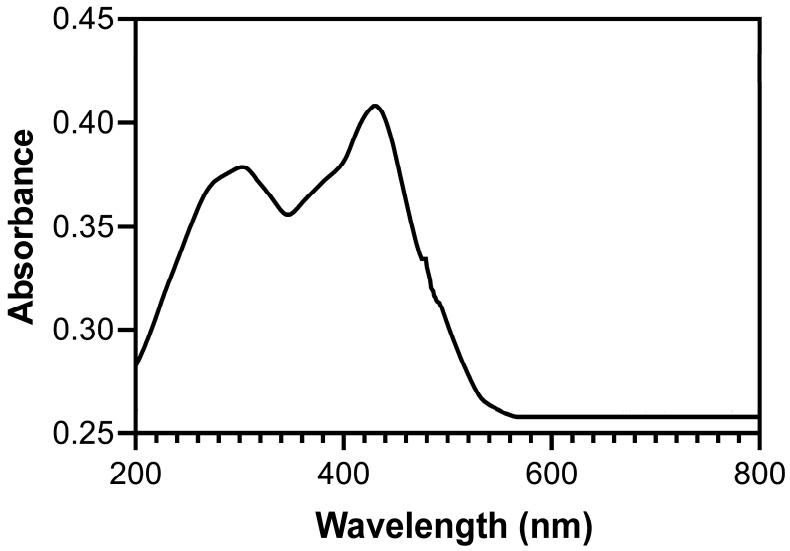

Figure 2. UV absorption spectrum of Ag nanoparticles

The SEM image shows the normal hexagonal crystal of UCNPs (Fig. 3a) has defects on both ends and sides, whereas the hexagonal crystal of Ag-UCNPs (Fig. 3b) doped with Ag is smooth. This smooth crystal structure then increases luminous intensity, and this view was confirmed by comparing their luminous intensities. The elemental distribution characterized by mapping confirms the successful doping of Ag nanoparticles (Fig. 4).

 doi:10.20944/preprints202111.0456.v1

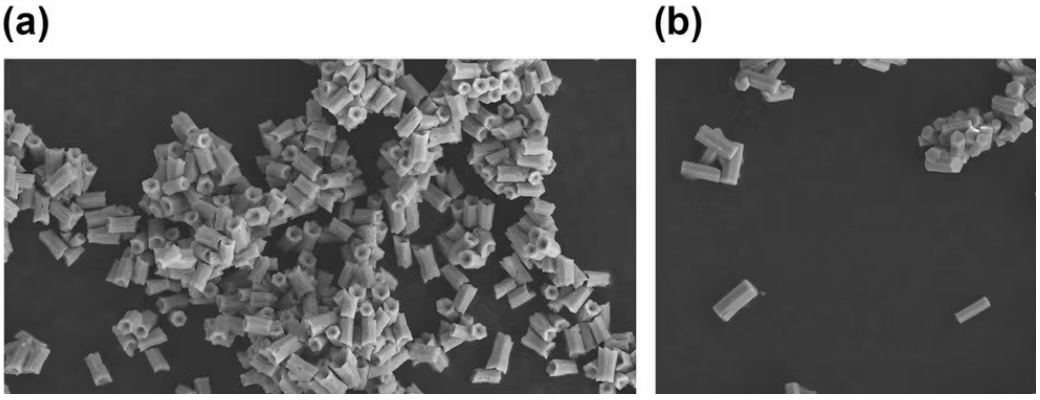

Figure 3. SEM image of UCNPs (a) and Ag-UCNPs (b)

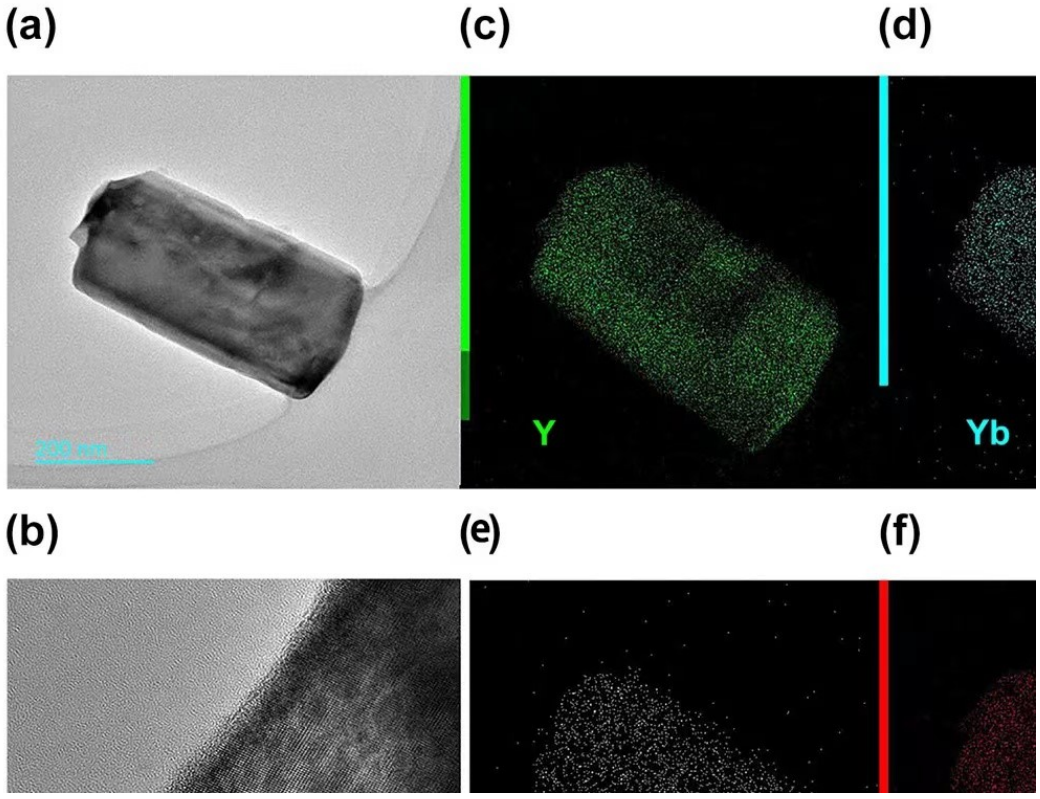

Figure 4. (a):TEM image of Ag-UCNPs, (b): Lattice of Ag-UCNPs, (c-f):mapping of (a)

Both UCNPs and Ag-UCNPs were prepared in 0.2 M solutions and their luminescence intensity (Fig. 5) at a wavelength of 980 nm was tested. The results demonstrated that the luminescence intensity increased by ~6.5 times after doping with Ag. This phenomenon can be explained using first-principles calculations.

Preprints (www.preprints.org) | NOT PEER-REVIEWED | Posted: 24 November 2021 doi:10.20944/preprints202111.0456.v1

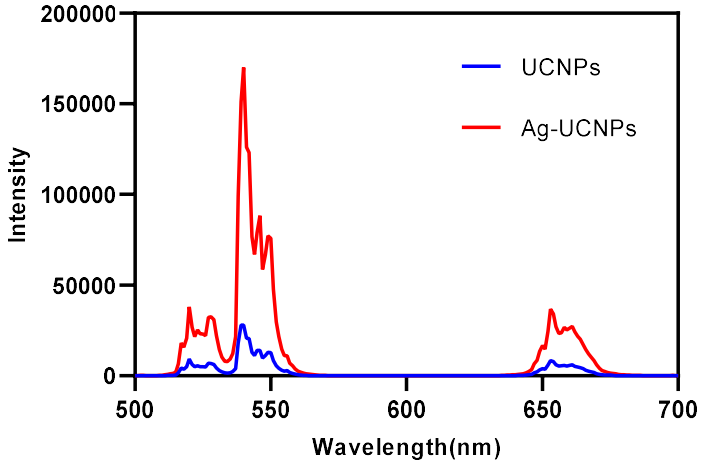

Figure 5. Luminescent intensity of UCNPs and Ag-UCNPs

DFT calculations were performed to understand the electronic properties and chemical origins of Ag nanoparticles better. We selected Ag-$NaYF_4$ to examine the effect of Ag nanoparticles on the Er luminescence center of materials because of the difficulty of convergence in multi-rare earth-doping systems. As shown in Fig. 5, the calculated total density of states (DOS) shows a considerable bandgap for pure $NaYF_4$. The bandgap is 6.78 eV, which corresponds to experimental values. The bandgap then narrows and additional hybridized electronic states occur close to the Fermi level in Ag-$NaYF_4$ when Ag nanoparticles are doped in Er-$NaYF_4$, (Fig. 6). The hybridized electronic states close to the Fermi level are shown to be formed by the 4f orbital of Er's 4d orbital of Ag and 2p orbital of F. The enhancement of total DOS close to the Fermi level in Ag-$NaYF_4$ may make it easier to absorb photons and enhance luminescence.

 doi:10.20944/preprints202111.0456.v1

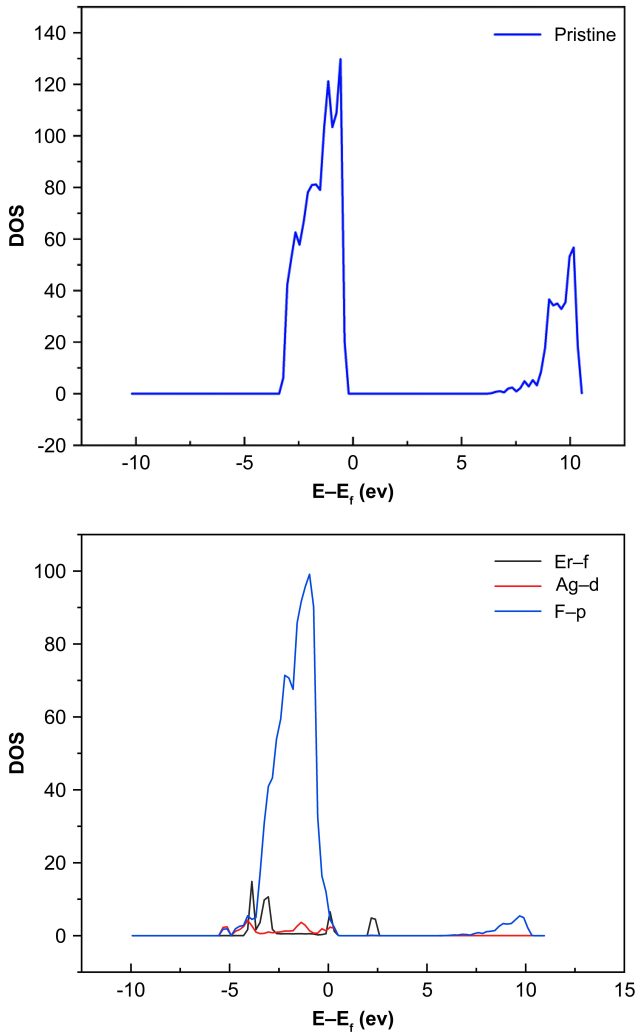

Figure 6. Computed DOS of the perfect $NaYF_4$ and Ag-$NaYF_4$ doping structures.

Although this luminescence intensity is sufficient for imaging organisms, it does not solve the bi-otoxicity problem (Fig. 6).

 doi:10.20944/preprints202111.0456.v1

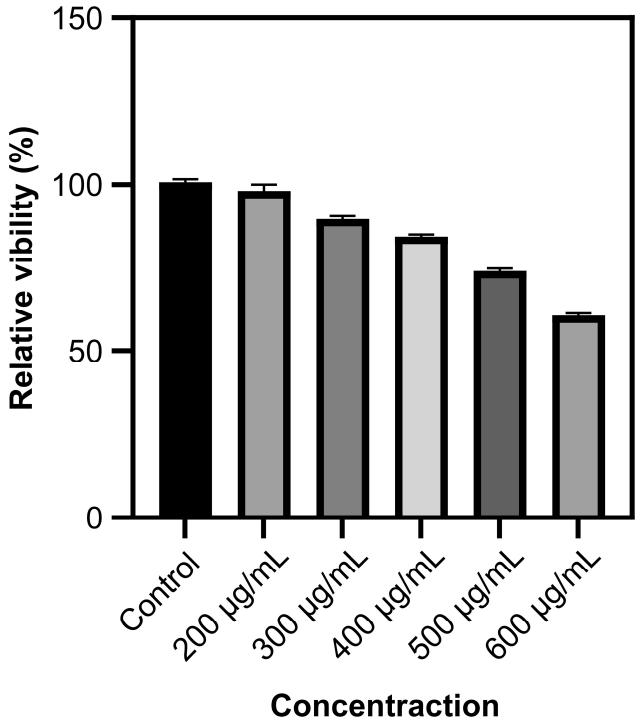

Figure 7. Cytotoxicity of different concentrations of Ag-UCNPs

A reverse microemulsion method was used to fabricate a SiO_2 shell structure coated with Ag-UCNPs. Moreover, TEM was used to confirm that SiO_2 successfully coated Ag-UCNPs (Fig. 8).

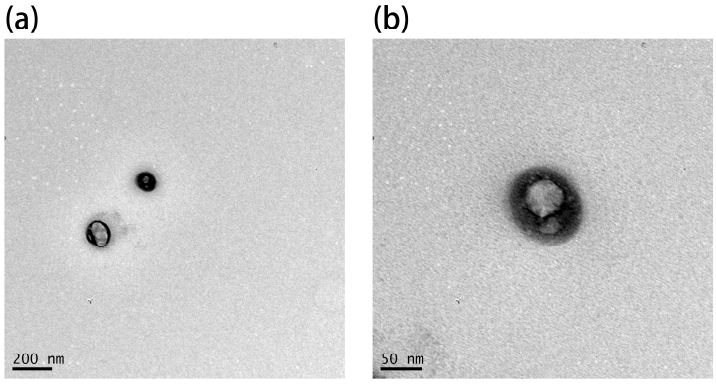

Figure 8. TEM image of Ag-UCNPs-SiO_2

Modified rare-earth nanomaterials were dispersed in normal saline to prepare different concentrations after which HeLa cells were cultured for 4 h and their activity was tested (Fig. 9). When the concentration is <400 μg/mL, the cell survival rate is >89%. In particular, at 200 μg/mL, the cell survival rate was >99%. Combined with Fig. 5, the luminescence intensity of rare earth, 200 μg/mL concentration of rare-earth nanomaterials not only have sufficient safety but also have a high luminous intensity. When the rare-earth ion concentration is as high as 500 or even 600 μg/mL, the cell survival rate is still >80%.

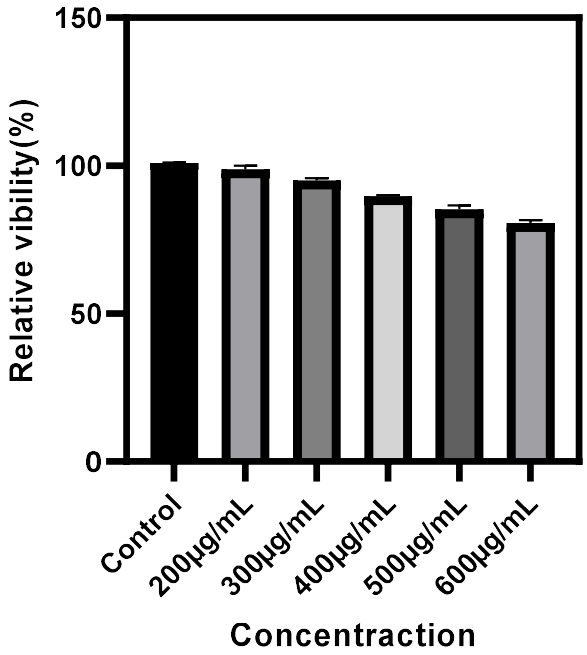

Figure 9 Cytotoxicity of different concentrations of Ag-UCNPs-SiO_2

A 200 μg/mL concentration of Ag-UCNPs-SiO_2 was intratumorally injected in the mice. Fig. 10(c) shows that the tumor site of the mouse before injection has no signal under Micro-CT imaging; furthermore, 30 min after the injection of Ag-UCNPs-SiO_2 (Fig. 10 d), the tumor site of the mouse shows a CT Signal.

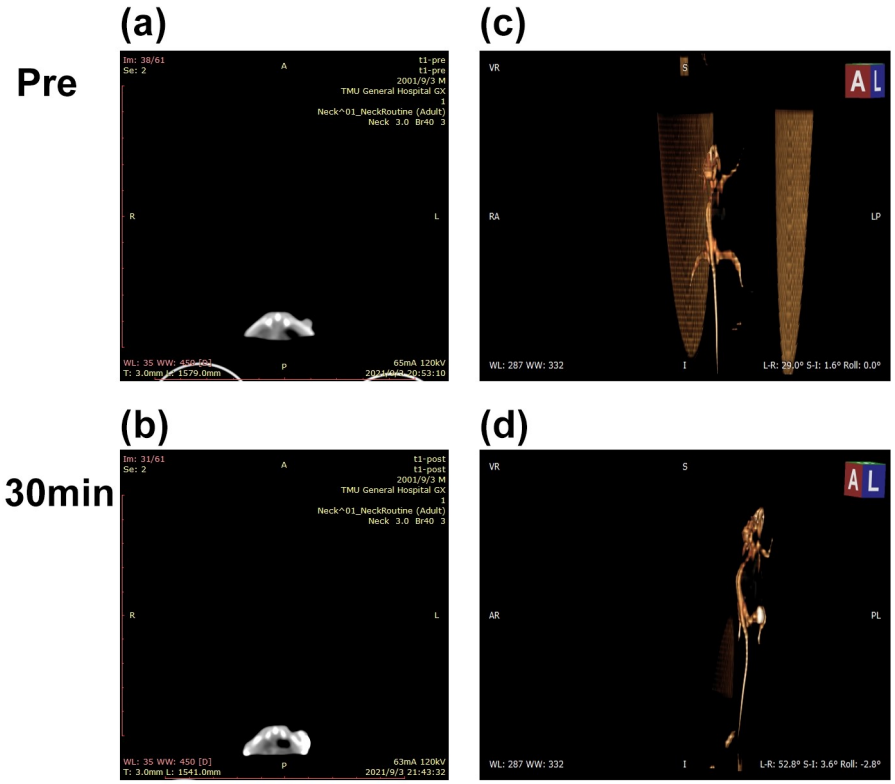

Figure 10 Micro-CT images before and after intratumor injection of Ag-UCNPs-SiO_2 in Balb/c mice

4. Conclusions

The doped Ag nanoparticles increase the luminous intensity of UCNPs, and SiO_2, which has excellent biocompatibility, was used as the shell material; it greatly improves the luminous intensity of up-conversion nano-materials and has extremely low cytotoxicity. These nanoparticles can be used as An excellent biomedical material. Second, compared with the traditional medical imaging, tumor images can be observed in the in-vivo single-mode imaging system. The images can play an important role in future multi-mode imaging systems, thus providing complete and clear images for diagnosing and treating complex cancers such as blood metastasis. Finally, the extremely high luminous intensity of this material is primarily attributed to Ag nanoparticles, which have good photothermal conversion efficiency. In future, this material could be used along with photothermal therapy (PTT) and multi-mode imaging, which is used to complete the cancer treatment and diagnosis.

Author Contributions: Conceptualization, W.Z. and Y.Z.; methodology, J.H.; software, Y.L.; validation, W.Z., Y.Z., and Y.L.; formal analysis, J.H.; resources, Q.X.; data curation, Q.X. and Y.L.; writing—original draft preparation, W.Z.; writing—review and editing, J.X.; supervision, J.X. All authors read and agreed to the published version of the manuscript.

Funding: This research received no external funding.

Institutional Review Board Statement: Not applicable.

Informed Consent Statement: Not applicable.

Data Availability Statement: No new data were created or analyzed in this study. Data sharing is not applicable to this article.

Acknowledgments: The authors also would like to thank the Shiyanjia Lab(www.shiyanjia.com , 8 2021) for animal experiment.

Conflicts of Interest: The authors declare no conflict of interest.

References

1. A.M. Alattar, R.A. Mohammed, M.J. Alwazzan, W.A.A. Twej, Dispersion of pure silica xerogel vs NaYF4- xerogel nanomaterials in silica aerogel and their effect on the optical and structural properties, Opt. Mater. 118 (2021) 111274. https://doi.org/10.1016/j.optmat.2021.111274.
2. A.A. Ansari, A.K. Parchur, N.D. Thorat, G.Y. Chen, New advances in pre-clinical diagnostic imaging perspectives of functionalized upconversion nanoparticle-based nanomedicine, Coordin. Chem. Rev. 440 (2021) 213971. https://doi.org/10.1016/j.ccr.2021.213971.
3. N. Chowdhury, N. Riesen, H. Riesen, Yb3+ and Er3+ codoped BaLiF3 nanocrystals for x-ray dosimetry and imaging by upconversion luminescence, ACS Appl. Nano Mater. 4 (2021) 6659–6667. https://doi.org/10.1021/acsanm.1c00600.
4. A. Cordonnier, D. Boyer, S. Besse, R. Valleix, R. Mahiou, M. Quintana, A. Briat, M. Benbakkar, F. Penault-Llorca, A. Maisonial-Besset, B. Maunit, S. Tarrit, M. Vivier, T. Witkowski, L. Mazuel, F. Degoul, E. Miot-Noirault, J.M. Chezal, Synthesis and in vitro preliminary evaluation of prostate-specific membrane antigen targeted upconversion nanoparticles as a first step towards radio/fluorescence-guided surgery of prostate cancer, J. Mater. Chem. B (2021). https://doi.org/10.1039/d1tb00777g.
5. L. Dong, C.Y. Zhang, L. Yan, B.B. Zhang, H. Chen, X.H. Mi, Z.K. Fu, Z.L. Zhang, H.R. Zheng, Quantifying plasmon resonance and interband transition contributions in photocatalysis of gold nanoparticle*, Chinese Phys. B 30 (2021) 077301. https://doi.org/10.1088/1674-1056/abfa0c.
6. Z.H. Feng, L. Lin, Z.Z. Wang, Z.Q. Zheng, Highly efficient and wide range low temperature sensing of upconversion luminescence of NaYF4: Er3+ nanoparticles: Effects of concentration of active or sensitive ions, excitation power and particle size on temperature sensing sensitivity, Opt. Commun. 491 (2021), 126942. https://doi.org/10.1016/j.optcom.2021.126942.
7. L. Giordano, M.F. Nunes, V.N.C. Teixeira, L.C.V. Rodrigues, Green synthesis of upconverting NaYF4 and NaGdF4 materials and energy levels determination, J. Braz. Chem. Soc. 32 (2021) 1552–1558. https://doi.org/10.21577/0103-5053.20210052.
8. J.M. Jiang, H.H. Ren, F.H. Huang, L. Wang, J.L. Zhang, Refine the crystallinity of upconversion nanoparticles for NIR-enhanced photocatalysis, Crystengcomm. (2021). https://doi.org/10.1039/D1CE00550B.
9. C.M.S. Jones, D. Biner, S. Misopoulos, K.W. Kramer, J. Marques-Hueso, Optimized photoluminescence quantum yield in upconversion composites considering the scattering, inner-filter effects, thickness, self-absorption, and temperature, Sci. Rep-Uk 11 (2021) 13910. https://doi.org/10.1038/s41598-021-93400-8.
10. H. Zong, X.J. Mu, M.T. Sun, Physical principle and advances in plasmon-enhanced upconversion luminescence, Appl. Mater. Today 15 (2019) 43-57. https://doi.org/10.1016/j.apmt.2018.12.015.
11. Y.B. Wang, W.X. Xu, L. Lei, L. Chen, R.G. Ye, S.Q. Xu, Photoluminescent NaGdF4@NaYF4:Ce/Tb inert-core/active-shell nanoparticles for selective and ultra-sensitive Cu2+ions sensing, J. Lumin. 235 (2021) 118024. https://doi.org/10.1016/j.jlumin.2021.118024.
12. F. Lu, T. Zhao, X.J. Sun, Z.Q. Wang, Q.L. Fan, W. Huang, Rare-earth doped nanoparticles with narrow NIR-II emission for optical imaging with reduced autofluorescence, Chem. Res. Chinese U 37 (2021) 943–950. https://doi.org/10.1007/s40242-021-1172-9.
13. M.K. Mahata, R. De, K.T. Lee, Near-infrared-triggered upconverting nanoparticles for biomedicine applications, Biomedicines 9 (2021) 756. https://doi.org/10.3390/biomedicines9070756.
14. G. Murali, S.V.P. Vattikuti, Y.K. Kshetri, H. Lee, J.K.R. Modigunta, C.S. Reddy, S. Park, S. Lee, B. Poornaprakash, H. Lee, Y.H. Park, J. Lee, S.Y. Park, I. In, Near-infrared-activated Z-scheme NaYF4:Yb/Tm@Ag3PO4/Ag@g-C3N4 photocatalyst for enhanced H2 evolution under simulated solar light irradiation, Chem. Eng. J. 421 (2021) 129687. https://doi.org/10.1016/j.cej.2021.129687.
15. S.S. Panikar, G. Ramirez-Garcia, N. Banu, A.A. Vallejo-Cardona, P. Lugo-Fabres, T.A. Camacho-Villegas, P. Salas, E. de la Rosa, Ligand-targeted theranostic liposomes combining methylene blue attached upconversion nanoparticles for NIR activated bioimaging and photodynamic therapy against HER-2 positive breast cancer, J. Lumin. 237 (2021) 118143. https://doi.org/10.1016/j.jlumin.2021.118143.
16. Y.H. Tai, Y. Zhang, J.L. Sun, F.Y. Liu, H.R. Tian, Q.F. Liu, C.H. Li, Y2O3:Yb3+, Tm3+/ZnO composite with a heterojunction structure and upconversion function for the photocatalytic degradation of organic dyes, RSC Adv. 11 (2021) 24044–24053. https://doi.org/10.1039/D1RA03066C.
17. Y. Tian, Q.H. Liu, E. Fei, R.G. Ye, S.T. Chen, J.J. Zhang, S.Q. Xu, Structural evolution, crystallization behaviour and mid-infrared emission properties in Yb/Ho codoped oxyfluoride germanosilicate glass ceramics with varied Si/Ge ratio, Infrared Phys. Techn. 116 (2021) 103741. https://doi.org/10.1016/j.infrared.2021.103741.

18. R.A. Puebla, N.P. Perez, L. Guerrini, SERS-fluorescent encoded particles as dual-mode optical probes, Appl. Mater. Today 13 (2018) 1-14. https://doi.org/10.1016/j.apmt.2018.07.007.
19. J.Y. Xiong, G. Li, J. Zhang, D.S. Li, E.Y.B. Pun, H. Lin, Fluorescence regulation derived from Eu3+ in miscible-order fluoride-phosphate blocky phosphor, Nanotechnology 32 (2021) 435705. https://doi.org/10.1088/1361-6528/ac15c7.
20. Y.H. Zhang, X.H. Zhu, J. Zhang, Y.H. Wu, J.L. Liu, Y. Zhang, Synergistic upconversion photodynamic and photothermal therapy under cold near-infrared excitation, J. Colloid. Interf. Sci. 600 (2021) 513–529. https://doi.org/10.1016/j.jcis.2021.05.017.